ELSEVIER

Chemical Engineering Journal 136 (2008) 364–372

Chemical Engineering Journal

www.elsevier.com/locate/cej

Multifractal detrended fluctuation analysis of pressure fluctuation signals in an impinging entrained-flow gasifier

Miaoren Niu *, Fuchen Wang, Qinfeng Liang, Guangsuo Yu, Zunhong Yu

Institute of Clean Coal Technology, East China University of Science & Technology, Meilong Rd No. 130, Shanghai 200237, PR China

Received 26 January 2007; accepted 19 April 2007

Abstract

On a laboratory-scale testing platform of impinging entrained-flow gasifier with two-burner, the pressure signals are measured at two axial positions with stainless steel water-cooled probes. The probes are traversed radially from the wall to the reactor centerline (spaced 15 cm apart) for six radial positions (0, 3, 6, 9, 12, and 15 cm) to acquire pressure signals. Multifractal detrended fluctuation analysis (MF-DFA) is a method which is accurate and easy to implement, therefore it is used on the pressure fluctuation to examine the multifractal characteristics. It is found that the pressure fluctuation exhibits multifractal characteristics, the analysis of the pressure fluctuation signals under "unstable operating state", "stable operating state" and also "cold state" suggests that the combustion system is characterized by a dynamical change from heterogeneity toward homogeneity, revealed by a loss of multifractality. Moreover, the analysis confirms the existence of multifractal characteristics in the investigated pressure fluctuation series. Origin of multifractal phenomena of the pressure signal measured in the entrained-flow gasifier is interpreted in terms of the multiplicative cascade process.

Keywords: Entrained-flow gasifier; Pressure fluctuation; Detrended fluctuation analysis

1. Introduction

Gasification is a very versatile process to convert a variety of carbon-containing feedstocks as coal, petroleum coke, lignite, heavy oils, residues and natural gas into syngas. The entrained-flow gasification technology has been extensively applied to the production of ammonia, methanol, acetic acid, other chemicals and also the power generation in Integrated Gasification Combined Cycle (IGCC) application [1–3]. The gasification process of an entrained-flow gasifier is very complicated, because it relates to the fluid flow under the condition of high temperature, high pressure and heterogeneous state. Use of impinging stream flow configurations, which are characterized by streams of jets of fluid impinging against each other in a confined vessel, has proved useful in conducting a wide array of chemical engineering unit operations and enhancing heat and mass transfer between phases due to the high transfer coefficients obtainable in this type of flow configuration [4–10]. A comprehensive literature review on various aspects of the opposing jet techniques and their applications has been presented by Kudra and Mujumdar [11], Michel [12], Kostiuk [13] and Tamir [14]. Two equal suspension streams flow against one another at high velocity (>35 m/s) and impinge at their midpoint, resulting in a highly turbulence zone. The gas flows decrease their axial velocity up to zero at the impingement plane, and then turn to radiant; while particles penetrate to and from between the opposed streams by inertia and friction forces, and achieve the highest relative velocity at the beginning of penetration.

Fractals and multifractals are ubiquitous in natural and social sciences [15]. The most usual records of observable quantities are in the form of time series and their fractal and multifractal properties have been extensively investigated. There are many methods proposed for this purpose [16,17], such as spectral analysis, rescaled range analysis (R/S analysis)[18], fluctuation analysis [19], detrended fluctuation analysis (DFA) [20–22], wavelet transform module maxima (WTMM) [23–25], and detrended moving average [26–28], to list a few. Due to the simplicity in implementation, the DFA is now becoming the most important method for determination of fractal scaling properties and detection of long-range correlations in noisy, nonstationary time series. It has been successfully applied to a number of classical study fields such as DNA sequences [29], neuron spiking [30], long-time weather records [31], geology [32–37], economics time series [38,39], texture analysis [40] and heart

* Corresponding author. Tel.: +86 21 64252831; fax: +86 21 64252521.
E-mail address: niumiaoren@yahoo.com.cn (M. Niu).

1385-8947/$ – see front matter © 2007 Elsevier B.V. All rights reserved.
doi:10.1016/j.cej.2007.04.022

Nomenclature

D_i	independent random variable, $0 < D_i \leq 1$
$f(\alpha)$	singularity spectrum; multifractal spectrum
Δf	the difference of fractal dimensions
F_0	the initial equipment factor
F_m	the final pressure fluctuation phenomenon
$F_q(s)$	the detrended fluctuation function
$F^2(v, s)$	the variance for each of the $2N_s$ segments
$h(q)$	a family of scaling exponents
ΔP	pressure difference (Pa)
q	the index variable, can take any real value
s	the size scale
x_k	a series of length N
$y_v(i)$	the fitting polynomial in the vth segment
$Y(i)$	the cumulative sum
$Y_s(i)$	the difference between the original time series and the fits

Greek letters

α	the singularity strength
$\Delta\alpha$	the width of multifractal spectrum
$\tau(q)$	the mass exponent

rate [41]. As a result, we choose this method to analyze our data.

The main objective of this paper is to investigate the multifractal characteristics of different pressure fluctuation signals in a gasifier using multifractal detrended fluctuation analysis (MF-DFA), and to judge different combustion status. The paper is organized as follows: Section 2 describes the MF-DFA in detail. Section 3 outlines the schematic diagram of experiment setup. Section 4 presents the results of data analysis and discusses their physical interpretation. Section 5 comments on the implications of the current work.

2. Multifractal detrended fluctuation analysis (MF-DFA)

The idea of DFA was invented originally to investigate the long-range dependence in coding and noncoding DNA nucleotide sequences [20]. Then it was generalized to study the multifractal nature hidden in time series, termed multifractal DFA (MF-DFA) [22]. Due to the simplicity in implementation, the DFA is now becoming the most important method in the field. The MF-DFA procedure consists of the following steps. Let us suppose that x_k is a series of length N, and this series is of compact support.

Step 1 Calculate the cumulative sum

$$Y(i) \equiv \sum_{k=1}^{i} [x_k - \langle x \rangle], \quad i = 1, \ldots, N \tag{1}$$

where $\langle x \rangle$ represents the average value.

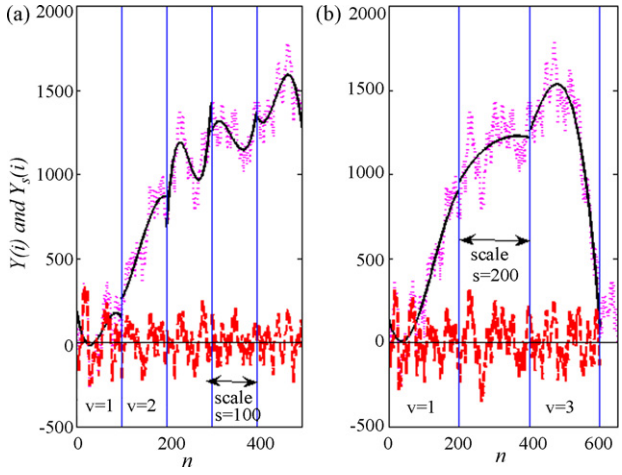

Fig. 1. Illustration of detrending procedure in the detrended fluctuation analysis: for two segment lengths $s = 100$ (a) and 200 (b), the profiles $Y(i)$ (dotted lines; defined in Eq. (1)), least squares quadratic fits to the profiles (solid lines), and the detrended profiles $Y_s(i)$ (dashed lines) are shown vs. the pressure fluctuation. One sees that the typical variance for a box in (a) is smaller than that in (b).

Step 2 Divide the profile $Y(i)$ into $N_s \equiv \text{int}(N/s)$ nonoverlapping segments of equal length s (see Fig. 1). Since length N of the series is often not a multiple of the considered scale s, a short part at the end of the profile may remain. In order not to disregard this part of the series, the same procedure is repeated starting from the opposite end. Thereby, $2N_s$ segments are obtained altogether.

Step 3 Calculate the local trend for each of the $2N_s$ segments by a least-square fit of the series. Then we define the detrended time series for segment duration s, denoted by $Y_s(i)$, as the difference between the original time series and the fits, $Y_s(i)$ represents the fluctuations with respect to the local average.

$$Y_s(i) = Y(i) - y_v(i) \tag{2}$$

$y_v(i)$ is the fitting polynomial in the vth segment. Fig. 1 illustrates this procedure for $s = 100$ and 200. In the example, quadratic polynomials are used in the fitting procedure, which is characteristic of quadratic DFA (DFA2). Linear, cubic, or higher order polynomials can also be used in the fitting procedure (conventionally called DFA1, DFA3, and higher order DFA). Then determine the variance for each of the $2N_s$ segments.

$$F^2(v, s) = \frac{1}{s}\sum_{i=1}^{s} \{Y[(v-1)s + i] - y_v(i)\}^2 = \frac{1}{s}\sum_{i=1}^{s} Y_s^2[(v-1)s + i] \tag{3}$$

for each segment v, $v = 1, \ldots, N_s$ and

$$F^2(v, s) = \frac{1}{s}\sum_{i=1}^{s} \{Y[N - (v - N_s)s + i] - y_v(i)\}^2 = \frac{1}{s}\sum_{i=1}^{s} Y_s^2[N - (v - N_s)s + i] \tag{4}$$

for $v = N_s + 1, \ldots, 2N_s$.

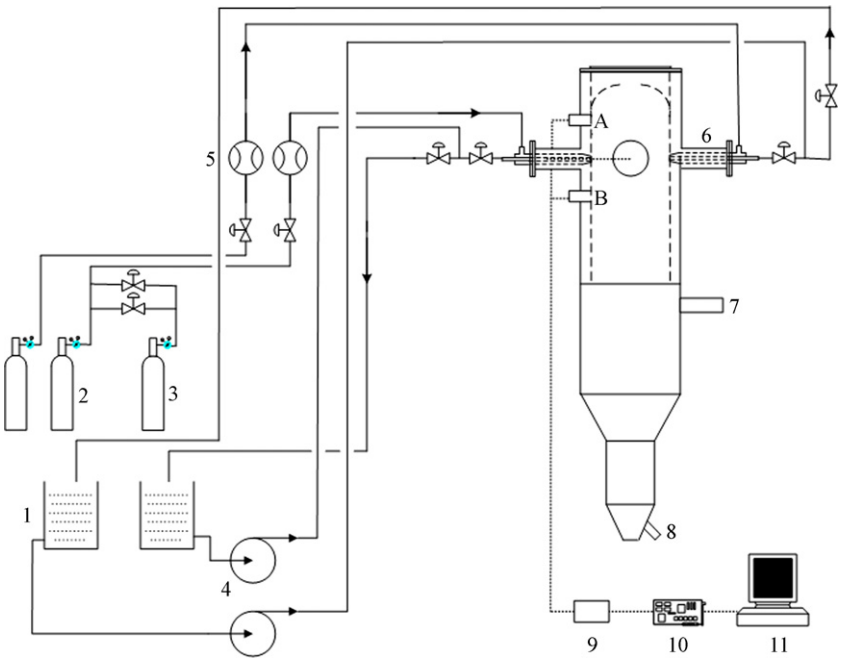

Fig. 2. Schematic diagram of experimental setup: 1, liquid tank; 2, O_2 steel cylinder; 3, N_2 steel cylinder; 4, pump; 5, gas mass flow meter; 6, burner; 7, syngas exit; 8, slag discharge; 9, pressure transducers; 10, A/D board; 11, computer.

Step 4 Average over all segments to obtain the qth order fluctuation function

$$F_q(s) \equiv \left\{ \frac{1}{2N_s} \sum_{v=1}^{2N_s} [F^2(v,s)]^{q/2} \right\}^{1/q} \tag{5}$$

where the index variable q can take any real value except for $q=0$. When $q=0$, we have

$$F_0(s) \equiv \exp\left\{ \frac{1}{4N_s} \sum_{v=1}^{2N_s} \ln[F^2(v,s)] \right\} \tag{6}$$

according to L'Hôpital's rule.

Step 5 Vary the value of s in the range from $s_{\min} \approx 6$ to $s_{\max} \approx N/4$, we can determine the scaling relation between the detrended fluctuation function $F_q(s)$ and the size scale s, which reads

$$F_q(s) \sim s^{h(q)} \tag{7}$$

Step 6 The final product of the MF-DFA procedure is a family of scaling exponents $h(q)$ which for actual multifractal signal form a decreasing function of q (for monofractals $h(q)=\text{const}$). From the $h(q)$ we can calculate the singularity spectrum $f(a)$ using the following relations:

$$a = h(q) + qh'(q), \quad f(a) = q[a - h(q)] + 1 \tag{8}$$

The shape and extension of $f(a)$-curve contains significant information about the distribution characteristics of the examined data set. In general, the spectrum has a concave downward curvature, with a range of a-values increasing correspondingly to the increase in the heterogeneity of the distribution. The width of multifractal spectrum is Δa ($\Delta a = a_{\max} - a_{\min}$) and the difference of fractal dimensions of maximum probability subset ($\alpha = a_{\min}$) and the minimum one ($\alpha = a_{\max}$) is Δf ($\Delta f = f(a_{\min}) - f(a_{\max})$). Δa and Δf can be either positive or negative.

3. Experimental

The schematic drawing of the experimental apparatus was shown in Fig. 2. The maximum values of operation pressure and temperature were 1 MPa and 1500 °C, respectively. The gasifier was cylindrical, vertically oriented, the inner diameter and length of the combustion chamber composed of a 15 mm thick cast refractory shell, were 300 and 2200 mm, respectively. The cast refractory shell, wrapped with a 235 mm thick, low thermal conductivity fiber blanket to reduce the heat transfer, was

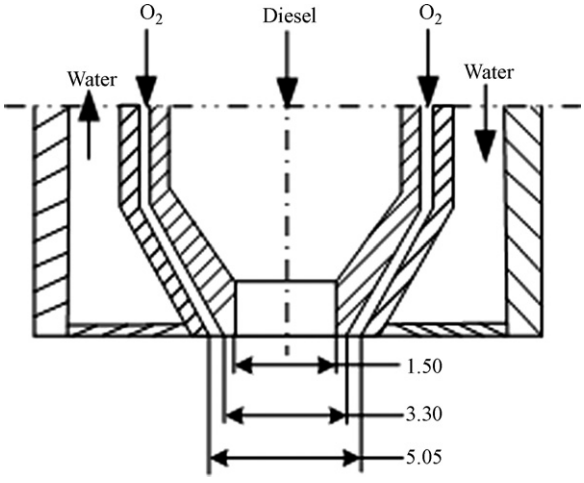

Fig. 3. General view of the burner (all dimensions in mm).

Table 1
Experimental conditions

Condition	1# diesel (kg/h)	2# diesel (kg/h)	1# O_2 (N m^3/h)	2# O_2 (N m^3/h)	O_2/fuel (N m^3/kg)	1# burner, velocity (m/s)	2# burner, velocity (m/s)
1	1.80	1.80	2.55	2.43	1.38	61.72	58.82
2	2.05	2.08	3.59	3.58	1.74	86.89	86.65
3	2.05	2.08	3.22	3.20	1.55	77.94	77.45
4	2.22	2.46	2.86	2.85	1.22	69.22	68.98
5	2.05	2.05	3.22	3.41	1.62	77.94	82.53
6	2.05	2.05	3.04	3.00	1.47	73.58	72.61
7	2.05	2.05	2.60	2.60	1.27	62.93	62.93
8	–	–	2.67	2.67	–	64.62	64.62

protected by a stainless steel column shell of 0.8 m in diameter and 2.5 m in height. Ports were located at sides of the gasifier for viewing, temperature measurement and insertion of the water-cooled probe. Opposed turbulent flow fields were obtained by two opposed round burners composed of inner and outer channels, which was shown in Fig. 3. The O_2 was fed into the burner outer channel by steel cylinder, with a pressure-reducing valve to avoid pressure oscillations in order to achieve steady flow. The gas flow rates were measured by mass flow meters (D07-9C/ZM, Beijing Sevenstar Huachuang Electronic Co., Ltd.). The diesel oil was fed into the burner inner channel by a gear pump (A-73004-00#, America Cole-Parmer Company), the flow rate was determined gravimetrically with an elapsed timer and an electronic weight scale. In the gasification process, two burners were used to produce opposite jets of fuel that impinge on the center of the combustion chamber. High relative velocities between the particulate matter and the gaseous phase in the central area provided good conditions for active diffusion and convection at the particle surface, and the high temperature together resulted in fast burning and gasification reaction under highly reducing conditions to produce raw syngas. High-temperature gaskets interfaced the furnace segments and eliminated all leakage. From the reaction chamber, the raw syngas flowed into the quench chamber, where the raw syngas was cooled and partially scrubbed by the water, then the syngas was discharged. After the experiment, the N_2 was fed into the burner inner channel by steel cylinder to clean burner.

Pressure signals were taken from the gasifier with two stainless steel water-cooled probes, at two axial positions equidistant from a burner, see positions A and B in Fig. 2, at each axial position, probe was traversed radially from the wall to reactor centerline (spaced 15 cm apart) for six radial positions (0, 3, 6, 9, 12, and 15 cm) to acquire pressure signals. A pressure sensor (CECC 420G22M1) was used to record the pressure fluctuations, the pressure sensor has two ports, one placed in combustion chamber and the other one (reference) kept at ambient pressure. Pressure difference ΔP were measured and then converted into voltage signals by a multi-channel card (PCI-1711L-A2). Voltage signals were sent to a computer to store results through an A/D converter. Pressure difference ΔP were used instead of static pressure signals, since differential pressure signals were much more stable and reliable compared to static pressure signals. Fourier analysis showed that the dominant frequency of the pressure fluctuation in the gasifier was lower than 40 Hz. Hence a sampling frequency of 100 Hz was chosen in the experiments. For each measurement, 20 000 points were recorded in order to include enough information. Pressure difference ΔP at the two axis positions were measured for all the experimental conditions. A summary of experimental conditions in this work was listed in Table 1.

4. Results and discussion

4.1. Calculation results

The pressure fluctuation signals' multifractal spectra $f(a)$ have been calculated for three states.

(1) Unstable operating state including ignition and shut down state.
(2) Stable operating state, due to the high thermal capacity of the refractory walls, about 4 h were needed to achieve steady state as monitored by steady readings of wall temperatures.
(3) Cold operating state, i.e. without flame but O_2 was still supplied to the burner outer channel by steel cylinder and the temperature of the gasifier was approximate indoor temperature.

Fig. 4 shows the first 10 000 typical pressure fluctuation signals in position A under condition 4 and the MF-DFA2 fluctuation functions $F_q(s)$.

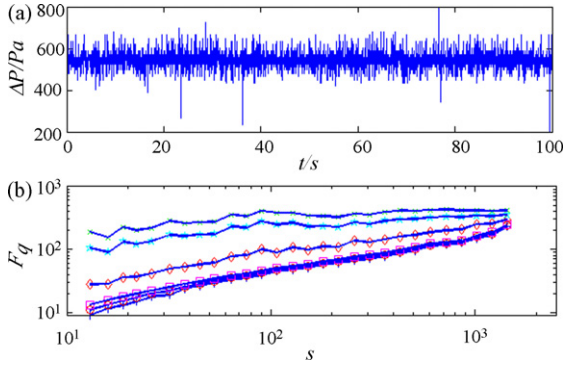

Fig. 4. The typical pressure fluctuation signals and the MF-DFA2 fluctuation functions $F_q(s)$: (a) typical pressure fluctuation signals for time series; (b) the MF-DFA2 fluctuation functions $F_q(s)$ vs. the scale s in log–log plots for the pressure fluctuation signals, symbols used to indicate the various moments are $q=6$ (×), $q=4$ (☆), $q=2$ (◊), $q=-2$ (□), $q=-4$ (◯), $q=-6$ (+).

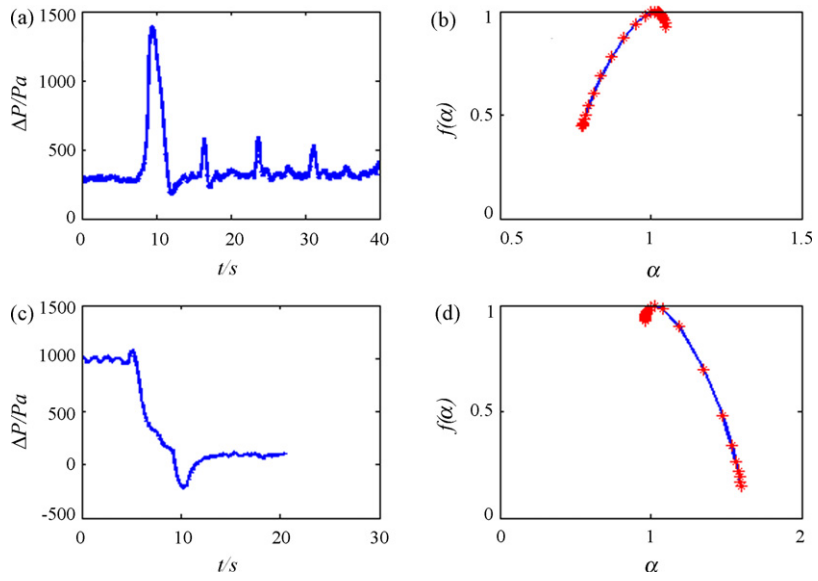

Fig. 5. The pressure fluctuation at unstable operating state: under condition 1, the ignition pressure fluctuation signals (a) and its multifractal spectrum (b); the shut down pressure fluctuation signals (c) and its multifractal spectrum (d).

Multifractal characteristics in different pressure fluctuation signals are confirmed by calculating the $\ln(F_q)$ versus $\ln(s)$ plots. Shown in Fig. 4(b) are plots of the qth-order moment F_q versus the scale s in a log–log plot. All of these plots are mostly close to be straight, have different slopes and are shown for comparison, signifying that the studied pressure fluctuation signals can be regarded as multifractal measures. Since multifractal characteristics indeed exist, the pressure fluctuation series may be transferred into a more useful compact form through the multifractal formalism, namely, the $f(a)$–a plots.

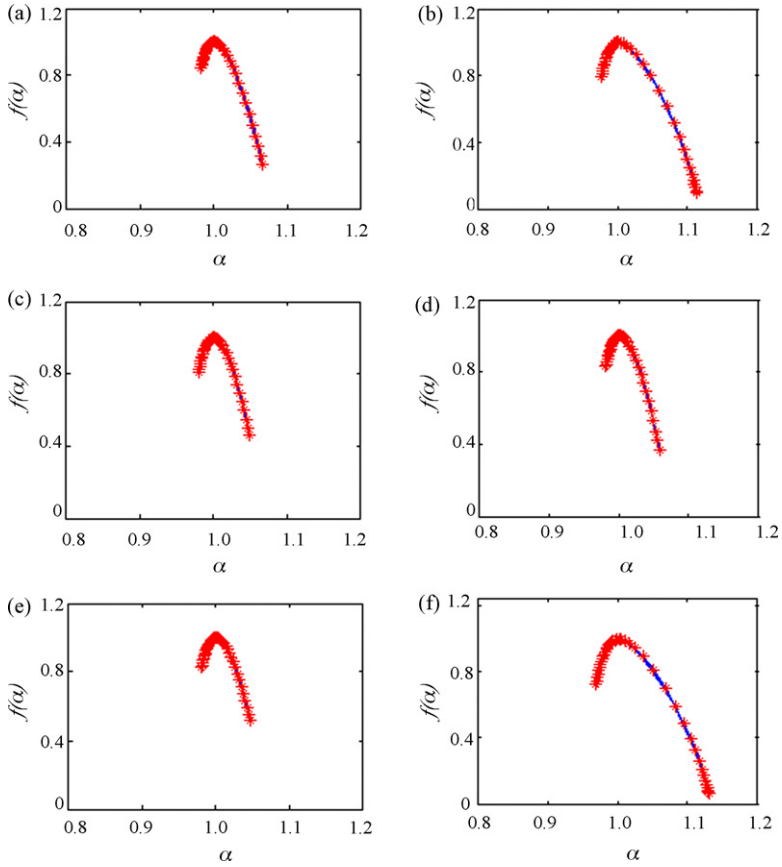

Fig. 6. The pressure fluctuation at stable operating state at axis position A: under condition 6, pressure fluctuation signals multifractality spectra in different radial positions are shown.

4.1.1. Unstable operating state

The multifractal spectra $f(a)$ of the pressure fluctuation signals for ignition and shut down are plotted in Fig. 5. It can be seen in Fig. 5 that different pressure fluctuation scopes and movement trends correspond to multifractal spectra with different sizes and shapes. Concretely, Fig. 5(a) denotes that the shape of multifractal spectrum is like a hook to the right (see Fig. 5(b)). On the contrary, Fig. 5(c) denotes that the shape of multifractal spectrum is like a hook to the left (see Fig. 5(d)). Intuitively, the multifractal spectra may contain some useful statistical information about the pressure movements.

In sum, Δa may indicate the absolute magnitude of the pressure movements in a gasifier, the larger value of Δa, the more violent of pressure fluctuation. The Δf may indicate the different trends of pressure movements. Multifractal spectrum is directly calculated from the pressure fluctuation signals, it should yield some information about the trend of different pressure fluctuation signals.

4.1.2. Stable operating state

Two equal suspension streams flow is against one another at high velocity (>35 m/s) and impinge at their midpoint, resulting symmetrical ascending and descending two zones. Axis positions A and B relatively near to the horizontal plane position of two burners, where the pressure fluctuation is more violent and the pressure signals is more abundant than other areas, under condition 6, we analyze the pressure fluctuations at two axis positions A and B, respectively. As is shown in Fig. 6, we can get Table 2, immediately.

Table 2
Values of $\Delta\alpha$ and Δf at axis position A

Insert (cm)						
	0 (a)	3 (b)	6 (c)	9 (d)	12 (e)	15 (f)
$\Delta\alpha$	0.0832	0.1365	0.0702	0.0768	0.0663	0.1628
Δf	0.5790	0.7006	0.3519	0.4625	0.3099	0.6621

As is shown in Table 2, under the stable rate of feed-in, for same axis position and different radial positions in the gasifier, $\Delta\alpha$ and Δf are not a constant. $\Delta\alpha$ has the maximum value at the center of the gasifier (Fig. 6(f)), Δf has the maximum value at probe insert 3 cm position (Fig. 6(b)), but at other radial positions, $\Delta\alpha$ and Δf have not obvious changing rules. $\Delta\alpha$ describes the singularity strength of some measure, the bigger $\Delta\alpha$ means the stronger singularity strength of the system more body multifractal characteristics and means the pressure signal fluctuation is more violent; Δf represents the changing trend of pressure fluctuations.

Because of two equal suspension streams that flow against one another and impinge at their midpoint, resulting in two zones namely symmetrical ascending and descending zones, the position (Fig. 6(f)) is at the ascending zones, which has the biggest gas velocity, and the fuel absorbs heat, inflates and

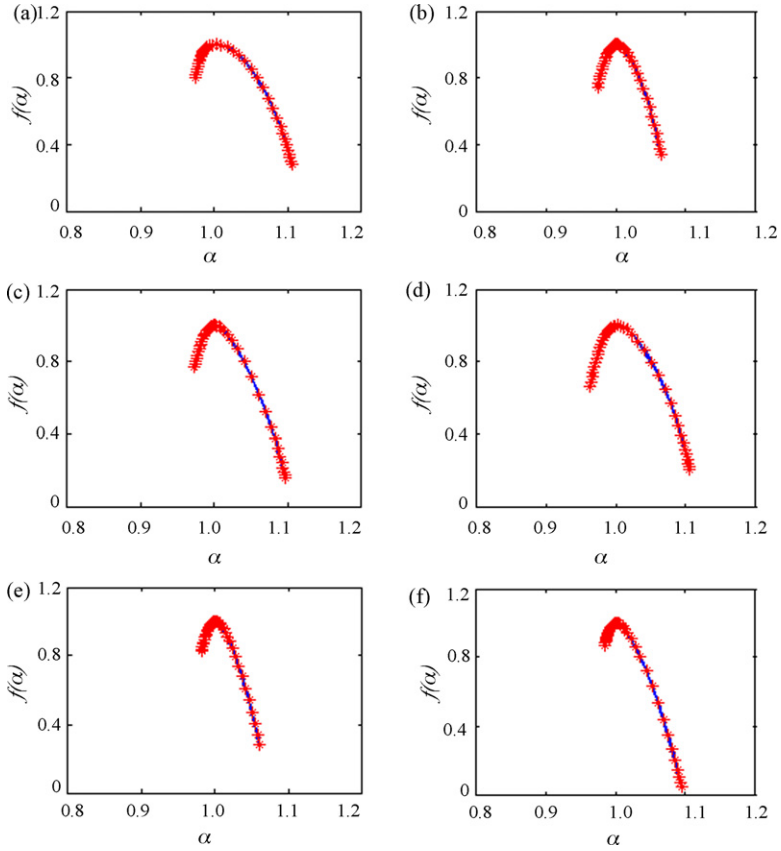

Fig. 7. The pressure fluctuation at stable operating state at axis position B: under condition 6, pressure fluctuation signals multifractality spectra in different radial positions are shown.

Table 3
Values of $\Delta\alpha$ and Δf at axis position B

Insert (cm)						
	0 (a)	3 (b)	6 (c)	9 (d)	12 (e)	15 (f)
$\Delta\alpha$	0.1318	0.0914	0.1233	0.1435	0.0794	0.1093
Δf	0.5218	0.4073	0.6102	0.4557	0.5391	0.8290

gasifies quickly; so this position is the most violent place of pressure fluctuation. $\Delta\alpha$ has the biggest value in this position and also means that the system has the most strong singularity strength in this position, which obvious shows the multifractal characteristics.

For position B, as is shown in Fig. 7, we can get Table 3, immediately.

As is shown in Table 3, under the stable rate of feed-in, for the same axis position and different radial positions in the gasifier, $\Delta\alpha$ and Δf are also not a constant. $\Delta\alpha$ has the maximum value at the probe insert 9 cm position (Fig. 7(d)), Δf has the maximum value at the center of the gasifier (Fig. 7(f)), but at other radial positions, both $\Delta\alpha$ and Δf have not obvious changing rules.

4.1.3. Compared the results of stable operating state with that of the cold state

Under the cold state, will the pressure fluctuation still show the multifractal characteristics? Therefore, we analyzed pressure fluctuation signals in different radial positions at axis position A, the result is shown in Fig. 8.

Fig. 8 shows the generalized fluctuation $F_q(s)$ for several q values. Although a slight q dependence is observable, all of these plots are mostly close to being parallel, signifying that the studied pressure fluctuation series under the cold state can be regard as monofractal measures. This confirmed that the actual reaction process in the combustion field is a high temperature, multiphase reaction, the absorbing heat and emitting heat of the flame reached a dynamical balance, which producing pressure fluctuations cannot be observed under cold states.

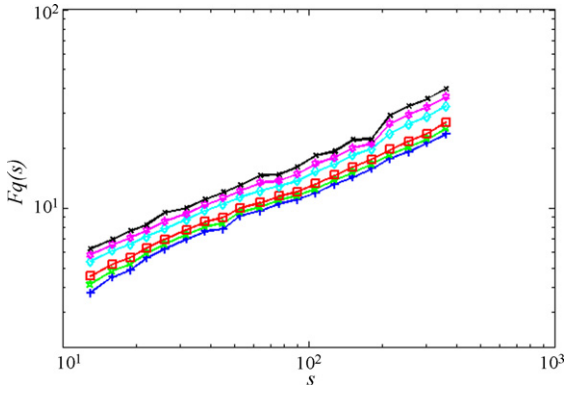

Fig. 8. The MF-DFA2 fluctuation functions $F_q(s)$ vs. the scale s in log–log plots for the cold state pressure fluctuation signals under condition 8 (insert 15 cm at axis position A): symbols used to indicate the various moments are $q=6$ (×), $q=4$ (☆), $q=2$ (◊), $q=-2$ (□), $q=-4$ (◯), $q=-6$ (+).

4.2. Discussion

Since the pressure fluctuation series distribution exhibits multifractal characteristics, then the next question is which processes lead to such multifractal characteristics, a physical interpretation must be done. When applying a multiscaling approach to temporal clustering of earthquakes, multifractal characteristics are interpreted in terms of diffusive processes of stress in the Earth's crust [42]. Moreover, multifractal characteristics in rainfall data have been explained with an assumption that a large-scale flux is successively broken into smaller and smaller cascades, each receiving an amount of the total flux specified by a multiplicative parameter [43]. On the other hand, the multifractal characteristics in air pollutant concentration time series are interpreted with the aid of random multiplicative process of air pollutant concentration [44,45]. It should be noted that the stochastic processes proposed for above systems to generate multifractal characteristics are closely related to the heart of turbulence, namely, the multiplicative cascade process. The only difference is the characteristic physical quantity accompanying in the stochastic processes. For earthquakes, rainfall, air pollutant and turbulence, the corresponding characteristic quantity is stress, water, concentration and energy, respectively. For pressure fluctuations, in practice, there is not just a single origin, the pressure signal measured in the gasifier is a result of a number of influencing factors, such as size and geometry of burner, physical properties of the dispersed phase and the continuous phase, the size of combustion chamber and operating state. Analysis of pressure measurements has indicated that the multifractal characteristics of these pressure fluctuations also depend on the temperature of the gasifier. Coal gasification generally refers to the reaction of coal with air, oxygen, steam, carbon dioxide, or a mixture of these gases to yield a gaseous product, this is a mol increased reaction and the reaction depends on temperature greatly. One mechanism by which energy can be transferred to an acoustic field was investigated by Lord Rayleigh [46], who stated the commonly cited criterion which follows:

"If heat be given to the air at the moment of greatest condensation, or be taken from it at the moment of greatest rarefaction, the vibration is encouraged. On the other hand, if heat be given at the moment of greatest rarefaction, or abstracted at the moment of greatest condensation, the vibration is discouraged". As a corollary to Rayleigh's criterion, we may state that if equal amounts of heat are added in and out of phase with the pressure oscillations, then the vibration is neither encouraged nor discouraged by the heat addition.

Due to the complexity of the atomization process, although it is difficult to clearly describe the mechanism and also impossible to combine all the influencing factors, but the two concepts, structural and operating factors, are found to be very useful in the description of pressure fluctuation processes. As mentioned earlier, multifractal behavior is frequently associated with systems where the underlying physics is governed by a random multiplicative process. So if we assume the multifractal characteristics of pressure fluctuation in the gasifier are generated through the random multiplicative process of all kinds of phenomena, the

final phenomenon F_m can be expressed by

$$F_m = F_0 D_1 D_2 \cdots D_m = F_0 \prod_{i=1}^{m} D_i \tag{9}$$

$$\ln F_m = \ln F_0 + \sum_{i=1}^{m} \ln D_i \tag{10}$$

where D_i is an independent random variable denoting the operating factor such that $0 < D_i \leq 1$, and F_0 is the initial equipment factor. As m approaches infinity, based on the central limit theorem (CLT), $\ln F_m$ will approach a normally distributed random variable plus a constant. In other words, the pressure fluctuation series will be lognormally distributed. The physical interpretation of the pressure fluctuation distributions using the above process seems to be acceptable to explain the multifractality.

5. Conclusions

On a laboratory-scale testing platform of impinging entrained-flow gasifier with two-burner, the pressure signals are measured at two axial positions with stainless steel water-cooled probes, probes are traversed radially from the wall to reactor centerline (spaced 15 cm apart) for six radial positions (0, 3, 6, 9, 12, and 15 cm) to acquire pressure signals. Multifractal detrended fluctuation analysis (MF-DFA) is a method which is accurate and easy to implement, therefore it is used on the pressure fluctuation to examine the multifractal characteristics. In conclusion, the pressure fluctuation signals are complex but not totally an uncorrelated random process. The observation of multifractal spectrum of pressure fluctuation in gasifier is encouraging since multifractal formalism has been successfully applied to systems as complex as turbulence, and has led to a better understanding of such complexity. The analysis of the pressure fluctuation signals under "unstable operating state", "stable operating state" and also "cold state" suggests that the combustion system is characterized by a dynamical change from heterogeneity toward homogeneity, which revealed by a loss of multifractality. The potential of multifractal analysis is far from being fully exploited, since it was only recently that attention has been drawn to the need for a thorough testing of the multifractal tools, and, in particular, a much deeper understanding of the nature of the impinging combustion phenomena and their interactions with the multifractal methods.

Finally, we would like to stress that there are tremendous potential applications of the MF-DFA in the analysis of fractals and multifractals. In the two-dimensional case, the methods can be adapted to the investigation of the roughness of fracture surface, flame images and many other images possessing self-similar properties. In the case of three dimensions, it could be utilized to quality the multifractal nature of temperature fields and concentration fields. So it may also have a great potential in modeling the complex structure of combustion field, concrete applications will be reported elsewhere in future presentations.

Acknowledgements

This work was partially supported by the National Basic Research Program of China (No. 2004CB217703), Shanghai Shuguang Training Program for the Talents (06SG34), and the Program for New Century Excellent Talents in University (NCET–05–0413).

References

[1] J.D.D. Graaf, Q. Chen, D. Haag, An update on Shell licensed gasification projects and performance of Pernis IGCC Plant, in: Presented at 2000 Gasification Technologies Conference, San Francisco, CA, October 8–11, 2000.
[2] J.T.G.M. Eurlings, J.E.G. Ploeg, Process performance of the SCGP at Buggenum IGCC, in: Presented at Gasification Technologies Conference, San Francisco, CA, October 18–20, 1999.
[3] W.E. Preston, The Texaco gasification process in 2000 startups and objectives, in: Presented at 2000 Gasification Technologies Conference, San Francisco, CA, October 8–11, 2000.
[4] N.S. Nosseir, S. Behart, Characteristics of jet impingement in a side-dump combustor, AIAA J. 24 (1986) 1752–1757.
[5] T.M. Liou, Y.Y. Wu, Turbulent flows in a model SDR combustor, J. Fluid Eng.-Trans. ASME 115 (1993) 468–473.
[6] Y. Berman, A. Tamir, Experimental investigation of phosphate dust collection in impinging streams (IS), Can. J. Chem. Eng. 74 (1996) 817–821.
[7] Y. Berman, A. Tanklevsky, Y. Oren, A. Tamir, Modeling and experimental studies of SO_2 absorption in coaxial cylinders with impinging streams, Part I, Chem. Eng. Sci. 55 (2000) 1009–1021.
[8] Y. Berman, A. Tanklevsky, Y. Oren, A. Tamir, Modeling and experimental studies of SO_2 absorption in coaxial cylinders with impinging streams, Part II, Chem. Eng. Sci. 55 (2000) 1023–1028.
[9] X. Hu, D. Liu, Experimental investigation on flow and drying characteristics of a vertical and semi-cyclic combined impinging streams dryer, Dry. Technol. 17 (1999) 1879–1982.
[10] A.M. Dehkordi, Application of a novel-opposed-jets contacting device in liquid–liquid extraction, Chem. Eng. Process. 41 (2002) 251–258.
[11] T. Kudra, A.S. Mujumdar, Impingement stream dryers for particle and pastes, Dry. Technol. 7 (1989) 219–266.
[12] M. Champion, P.A. Libby, Reynolds stress description of opposed and impinging turbulent jets. Part I. Closely spaced opposed jets, Phys. Fluids A 5 (1993) 203–215.
[13] L.W. Kostiuk, P.A. Libby, Comparison between theory and experiments for turbulence in opposed streams, Phys. Fluids A 5 (1993) 2301–2303.
[14] A. Tamir, Impinging-Stream Reactors, Fundamentals and Applications, Elsevier, Amsterdam, 1994.
[15] B.B. Mandelbrot, The Fractal Geometry of Nature, Freeman, New York, 1983.
[16] M. Taqqu, V. Teverovsky, W. Willinger, Estimators for long-range dependence, an empirical study, Fractals 3 (1995) 785–798.
[17] A. Montanari, M.S. Taqqu, V. Teverovsky, Estimating long-range dependence in the presence of periodicity, an empirical study, Math. Comput. Model. 29 (1999) 217–228.
[18] H.E. Hurst, Long-term storage in reservoirs, an experimental study, Trans. Am. Soc. Civ. Eng. 116 (1951) 770–808.
[19] C.K. Peng, S.V. Buldyrev, A.L. Goldberger, S. Havlin, F. Sciortino, M. Simons, H.E. Stanley, Long-range correlations in nucleotide sequences, Nature 356 (1992) 168–170.
[20] C.K. Peng, S.V. Buldyrev, S. Havlin, M. Simons, H.E. Stanley, A.L. Goldberger, Mosaic organization of DNA nucleotides, Phys. Rev. E 49 (1994) 1685.
[21] K. Hu, P.C. Ivanov, Z. Chen, P. Carpena, H.E. Stanley, Effect of trends on detrended fluctuation analysis, Phys. Rev. E 64 (2001) 011114.
[22] J.W. Kantelhardt, S.A. Zschiegner, E. Koscielny-Bunde, S. Havlin, A. Bunde, H.E. Stanley, Multifractal detrended fluctuation analysis of nonstationary time series, Physica A 316 (2002) 87–114.

[23] M. Holschneider, On the wavelet transformation of fractal objects, J. Stat. Phys. 50 (1988) 953–993.
[24] J.F. Muzy, E. Bacry, A. Arneodo, Wavelets and multifractal formalism for singular signals, Application to turbulence data, Phys. Rev. Lett. 67 (1991) 3515–3518.
[25] J.F. Muzy, E. Bacry, A. Arneodo, Multifractal formalism for fractal signals, the structure–function approach versus the wavelet-transform modulus-maxima method, Phys. Rev. E 47 (1993) 875–884.
[26] A. Carbone, G. Castelli, H.E. Stanley, Time-dependent Hurst exponent in financial time series, Physica A 344 (2004) 267–271.
[27] A. Carbone, G. Castelli, H.E. Stanley, Analysis of clusters formed by the moving average of a long-range correlated time series, Phys. Rev. E 69 (2004) 026105–26114.
[28] L. Xu, P.C. Ivanov, K. Hu, Z. Chen, A. Carbone, H.E. Stanley, Quantifying signals with power-law correlations, a comparative study of detrended fluctuation analysis and detrended moving average techniques, Phys. Rev. E 71 (2005) 051101–51114.
[29] S.V. Buldyrev, N.V. Dokholyan, A.L. Goldberger, S. Havlin, C.K. Peng, H.E. Stanley, G.M. Viswanathan, Analysis of DNA sequences using methods of statistical physics, Physica A 249 (1998) 430–438.
[30] S. Blesic, S. Milosevic, D. Stratimirovic, M. Ljubisavljevic, Detrended fluctuation analysis of time series of a firing fusimotor neuron, Physica A 268 (1999) 275–282.
[31] K. Ivanova, M. Ausloos, Application of the detrended fluctuation analysis (DFA) method for describing cloud breaking, Physica A 274 (1999) 349–354.
[32] L. Telesca, V. Lapenna, M. Macchiato, Multifractal fluctuations in seismic interspike series, Physica A 354 (2005) 629–640.
[33] R.G. Kavasseri, R. Nagarajan, A multifractal description of wind speed records, Chaos Soliton Fract. 24 (2005) 165–173.
[34] N. Vandewalle, M. Ausloos, P. Boveroux, The moving averages demystified, Physica A 269 (1999) 170–176.
[35] L. Telesca, V. Lapenna, M. Macchiato, Mono- and multi-fractal investigation of scaling properties in temporal patterns of seismic sequences, Chaos Soliton Fract. 19 (2004) 1–15.
[36] V. Lapenna, G. Martinelli, L. Telesca, Long-range correlation analysis of earthquake-related geochemical variations recorded in Central Italy, Chaos Soliton Fract. 21 (2004) 491–500.
[37] L. Telesca, G. Colangelo, V. Lapenna, M. Macchiato, Fluctuation dynamics in geoelectrical data, an investigation by using multifractal detrended fluctuation analysis, Phys. Lett. A 332 (2004) 398–404.
[38] J. Kwapien, P. Oswiecimka, S. Drozdz, Components of multifractality in high-frequency stock returns, Physica A 350 (2005) 466–474.
[39] P. Norouzzadeh, G.R. Jafari, Application of multifractal measures to Tehran price index, Physica A 356 (2005) 609–627.
[40] J. Alvarez-Ramirez, E. Rodriguez, I. Cervantes, J.C. Echeverria, Scaling properties of image textures, a detrending fluctuation analysis approach, Physica A 361 (2006) 677–698.
[41] P.A. Ritto, J.J. Alvarado-Gil, J.G. Contreras, Scaling and wavelet-based analyses of the long-term heart rate variability of the Eastern Oyster, Physica A 349 (2005) 291–301.
[42] C. Godano, M.L. Alonzo, G. Vilardo, Multifractal approach to time clustering of earthquakes application to Mt. Vesuvio seismicity, Pure Appl. Geophys. 149 (1997) 375–390.
[43] J. Olsson, J. Niemczynowicz, Multifractal analysis of daily spatial rainfall distributions, J. Hydrol. 187 (1996) 29–43.
[44] C.K. Lee, Multifractal characteristics in air pollutant concentration time series, Water Air Soil Pollut. 135 (2002) 389–409.
[45] C.K. Lee, D.S. Ho, C.C. Yu, C.C. Wang, T.H. Hsiao, Simple multifractal cascade model for the air pollutant concentration time series, Environmetrics 14 (2003) 255–269.
[46] L. Rayleigh, The Theory of Sound, Dover Publications, New York, 1945.